A combined model for {311} defect and dislocation loop evolution: Analytical formulation of kinetic precipitation model

Alp H. Gencer
Avant! Corporation, Wellesley, Massachusetts

Scott T. Dunham
Department of Electrical Engineering, University of Washington, Seattle, Washington

(Received 3 April 2001; accepted for publication 30 November 2001)

Accurate modeling of extended defect kinetics is of primary importance for prediction of transient enhanced diffusion (TED) following ion implantation of silicon. Our previously developed moment-based model [Gencer and Dunham, J. Appl. Phys. **81**, 631 (1997)] accurately accounts for formation and evolution of {311} defects and can be used to predict TED under subamorphizing conditions. Using experimental knowledge about the distribution of the {311} defect population, and making approximations on the sums that are encountered in the model, we are able to simplify this model. We demonstrate that these simplifications don't affect the predictive capabilities of the model for {311} defect kinetics and TED. Furthermore, we are able to extend the model, under the same simplifying assumptions, to account for dislocation loop formation from {311} defect unfaulting and dislocation loop evolution, giving a unified model for interstitial aggregation in silicon. The resulting analytical model does not impose any computational speed penalty when the loop extension is turned on, making it applicable to a wide range of problems. © *2002 American Institute of Physics.* [DOI: 10.1063/1.1446223]

I. INTRODUCTION

It is well accepted that interstitial agglomerates, namely {311} defects and dislocation loops, play the central role in transient enhanced diffusion (TED) following ion implantation of silicon. By controlling point defect concentrations, the formation, evolution, and transformation of these defects determine the total movement of the dopant profiles. Physically based, and yet computationally efficient models are needed to accurately simulate extended defect kinetics and TED.

In our previous work,[1] we developed a physically based model for simulating the kinetics of extended defect formation and dissolution (kinetic precipitation model) and also developed a computationally efficient version of the model based on the evolution of the moments of the extended defect size distribution (reduced kinetic precipitation model or RKPM).[2] However, even the efficient model required the calculation of a large lookup table, which led to speed and stability problems. In this article, we present a more efficient moment-based model which addresses these issues. At the same time, we extend the model to account for dislocation loop formation and evolution, thereby allowing the accurate simulation of nucleation, growth, transformation, and dissolution of self-interstitial aggregates following high dose and high-energy implants.

II. MOMENT-BASED MODEL FOR EXTENDED DEFECTS

Evolution of an extended defect population can be modeled by explicitly considering aggregates of different sizes as independent species and accounting for their kinetics by considering the attachment and emission of solute atoms.[1] We define f_n as the number of aggregates of size n per unit volume. The net rate of transformation from size n to $n+1$, may be written as

$$I_n = D\lambda_n (C_I f_n - C_{ss}\hat{C}_n^* f_{n+1}), \tag{1}$$

where D is the solute (interstitial) diffusivity, λ_n is a kinetic rate factor which can be determined from the geometry of the defects and the interface reaction rate, C_I is the solute (interstitial) concentration, f_n is the density per unit volume of clusters of size n, C_{ss} is the "solid solubility" associated with a reference structure (usually an infinitely large precipitate), and $\hat{C}_n^*$ is a reverse rate constant which can be determined from the excess surface and strain energy (ΔG_n^{exc}) associated with finite-size defects (relative to reference structure).[1] In this system, the free-energy change associated with the formation of a precipitate of size n from free solute atoms is given by

$$\Delta G_n = nkT \ln\left(\frac{C_I}{C_{ss}}\right) + \Delta G_n^{exc}, \tag{2}$$

which gives

$$\hat{C}_n^* = \exp\left(\frac{\Delta G_{n+1}^{exc} - \Delta G_n^{exc}}{kT}\right). \tag{3}$$

$\hat{C}_n^*$ represents the ratio between the solute concentrations at equilibrium with a finite-size precipitate and with the reference precipitate.

To reduce the number of solution variables, we follow the moment-based approach[2] and keep track of only the lowest order *moments* of the distribution ($m_i = \Sigma_{n=2}^{\infty} n^i f_n$, where $i = 0,1,2,\ldots$). The system of equations is then reduced to

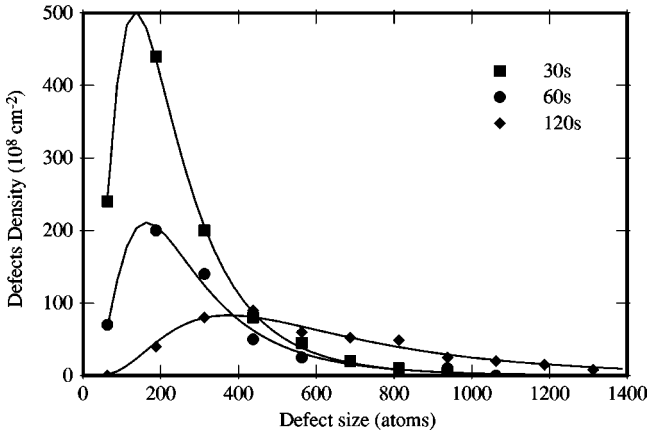

FIG. 1. Distribution of {311} defect densities over defect sizes and best fit to log−normal distribution. $z_2=0.8$ has been used in all fits. Data from Pan and Tu (see Ref. 3).

$$\frac{\partial m_i}{\partial t}=2^i I_1+\sum_{n=2}^{\infty}[(n+1)^i-n^i]I_n. \tag{4}$$

Since no finite number of moments can fully describe a complete distribution, we need a closure assumption, which is an assumption about the form of the distribution, $f_n=f(n,z_i)$, where z_i represent a set of parameters that characterize the distribution. In cases where we have no *a priori* knowledge about the distribution of defect sizes, we have used an energy-minimizing closure assumption.[1] We simply argued that the size distribution will be the one that minimizes the free energy given the moments, as found from constrained minimization of the free energy (ΔG_n). This results in the following distribution with three parameters, and hence a three-moment model (3KPM),

$$f_n=z_0\exp(-\Delta G_n^{\mathrm{exc}}/kT+z_1 n+z_2 n^2). \tag{5}$$

For {311} defects and dislocation loops, the size distribution has been measured experimentally.[3] The results suggest that the distribution is roughly log normal:

$$f_n=z_0\exp[-\ln(n/z_1)^2/z_2]. \tag{6}$$

Pan and Tu noted that the breadth of the size distributions they observed scales with the average size.[3] In accordance with this, we find that a constant value of z_2 ($z_2=0.8$) matches all the size distributions, independent of annealing time (Fig. 1). Thus, we can reduce the number of parameters (and hence also the number of moments) to 2. The resulting system is a two-moment system (2KPM):

$$\begin{aligned}
&\frac{\partial m_0}{\partial t}=I_1=D\lambda_1[C_I^2-C_{\mathrm{ss}}\hat{C}_1^* f_2],\\
&\frac{\partial m_1}{\partial t}=2I_1+\sum_{n=2}^{\infty} I_n,\\
&=2D\lambda_1[C_I^2-C_{\mathrm{ss}}\hat{C}_1^* f_2]+D\left[C_I\sum_{n=2}^{\infty}\lambda_n f_n\right.\\
&\quad\left.-C_{\mathrm{ss}}\sum_{n=2}^{\infty}\lambda_n\hat{C}_n^* f_{n+1}\right],
\end{aligned} \tag{7}$$

$$\frac{\partial C_I}{\partial t}=-\frac{\partial m_1}{\partial t}.$$

Normalizing the defect population such that $\hat{f}_n=f_n/(\Sigma_{n=2}^{\infty}f_n)=f_n/m_0$, we get the following system:

$$\begin{aligned}
&\frac{\partial m_0}{\partial t}=I_1=D\lambda_1[C_I^2-m_0 C_{\mathrm{ss}}\gamma_0],\\
&\frac{\partial m_1}{\partial t}=2I_1+D\bar{\lambda}m_0[C_I-C_{\mathrm{ss}}\gamma_1],\\
&\frac{\partial C_I}{\partial t}=-\frac{\partial m_1}{\partial t},
\end{aligned} \tag{8}$$

with

$$\begin{aligned}
&\gamma_0=\hat{C}_1^*\hat{f}_2,\\
&\gamma_1=\sum_{n=2}^{\infty}\hat{C}_n^*\hat{f}_{n+1}\lambda_n/\bar{\lambda},\\
&\bar{\lambda}=\sum_{n=2}^{\infty}\lambda_n\hat{f}_n.
\end{aligned} \tag{9}$$

The system can further be simplified by noting that for {311} defects the geometry factor ($\bar{\lambda}$) is almost independent of the defect size for large defects,[4] since {311} defects grow primarily in one direction. Thus, we can replace $\bar{\lambda}$ with size-independent λ. For a log-normal distribution, the integral of the distribution function can be found analytically, and therefore the parameters of the distribution can be calculated from the moments by means of analytical functions. This eliminates the need for the lookup table and interpolation, giving speed and robustness advantages. However, γ_1 still needs to be calculated by numerical sums, which is an iterative process.

III. ANALYTICAL KINETIC PRECIPITATION MODEL (AKPM)

Note that in the above equations, $\hat{f}_n$ is based on the distribution function we assume, and can be determined fully if $\hat{m}_1=m_1/m_0$ is given. For example, if the distribution function is a geometric distribution function ($\hat{f}_n=z_0 z_1^n$), then the distribution can be determined by solving the following set of equations:

$$\begin{aligned}
&1=\sum_{n=2}^{\infty} z_0 z_1^n,\\
&\hat{m}_1=\sum_{n=2}^{\infty} n z_0 z_1^n.
\end{aligned} \tag{10}$$

The solution of this system gives

$$\begin{aligned}
&z_1=\frac{\hat{m}_1-2}{\hat{m}_1-1},\\
&z_0=\frac{1-z_1}{z_1^2}.
\end{aligned} \tag{11}$$

Hence the normalized distribution can be written in terms of $\hat{m}_1$:

$$\hat{f}_n = \frac{1}{\hat{m}_1 - 1}\left(\frac{\hat{m}_1 - 2}{\hat{m}_1 - 1}\right)^{n-2}. \tag{12}$$

Since we also assume a functional form for $\hat{C}_n^*$, the γ_i are uniquely defined if $\hat{m}_1$ is known. Thus, in fact, the γ_i are functions of $\hat{m}_1$, with the appropriate limits:

$$\gamma_0 = \gamma_0(\hat{m}_1), \quad \gamma_1 = \gamma_1(\hat{m}_1),$$
$$\lim_{\hat{m}_1 \to 2} \gamma_0 = \hat{C}_1^*, \quad \lim_{\hat{m}_1 \to 2} \gamma_1 = 0, \tag{13}$$
$$\lim_{\hat{m}_1 \to \infty} \gamma_0 = 0, \quad \lim_{\hat{m}_1 \to \infty} \gamma_1 = 1.$$

For every $\Delta G_n^{\mathrm{exc}}$ $\hat{f}_n$ pair, we can find a corresponding $\gamma_0(\hat{m}_1)$, $\gamma_1(\hat{m}_1)$ pair, and instead of using the parameters of $\Delta G_n^{\mathrm{exc}}$ as our fitting parameters, we can use corresponding parameters of $\gamma_0(\hat{m}_1)$ and $\gamma_1(\hat{m}_1)$ as fitting parameters.

To demonstrate this transformation, we use an example. For simplicity of arithmetic, assume that $\hat{C}_n^*$ is given by an exponential function $\hat{C}_n^* = ab^{n-1} + 1$. Also, assume that the size distribution is again geometrical as given by Eq. (12). Simply substituting these functions into the definition of γ_i yields

$$\gamma_0 = \frac{1+a}{\hat{m}_1 - 1},$$
$$\gamma_1 = \sum_{n=2}^{\infty} (ab^{n-1} + 1)\frac{1}{\hat{m}_1 - 1}\left(\frac{\hat{m}_1 - 2}{\hat{m}_1 - 1}\right)^{n-1}, \tag{14}$$
$$= \frac{\hat{m}_1 - 2}{\hat{m}_1 - 1}\left[\frac{ab}{\hat{m}_1(1-b) - 1 + b} + 1\right].$$

For {311} defects, we used a generalized polynomial approximation for the form of $\Delta G_n^{\mathrm{exc}}$ in our previous work:[1]

$$\Delta G_n^{\mathrm{exc}} = a_0 n^{\beta_0} + a_1 n^{\beta_1} \cdots. \tag{15}$$

Starting with this form of $\Delta G_n^{\mathrm{exc}}$ and the log-normal distribution of the defect sizes as given in Eq. (6), we calculate the corresponding $\gamma_0(\hat{m}_1)$, $\gamma_1(\hat{m}_1)$ pairs numerically. Figure 2 shows sets of calculated γ_i for different sets of coefficients for the generalized polynomial of $\Delta G_n^{\mathrm{exc}}$. Although it is possible to solve the log-normal form exactly in order to determine the parameters (z_0 and z_1) from the moments (m_0 and $\hat{m}_1$,) it is not possible to calculate the sum in γ_1 analytically with the assumed form of $\Delta G_n^{\mathrm{exc}}$. It is computationally much faster to be able to express the γ_i as analytic functions of $\hat{m}_1$ rather than using a numeric sum. Our calculations show that the results can be approximated by the following functions of $\hat{m}_1$:

$$\gamma_0(\hat{m}_1) = \frac{K_1}{\hat{m}_1 - 1},$$
$$\gamma_1(\hat{m}_1) = \frac{\hat{m}_1 - 2}{\hat{m}_1 + K_0}\left(1 + \frac{(K_0+2)K_2}{\hat{m}_1 + K_0}\right). \tag{16}$$

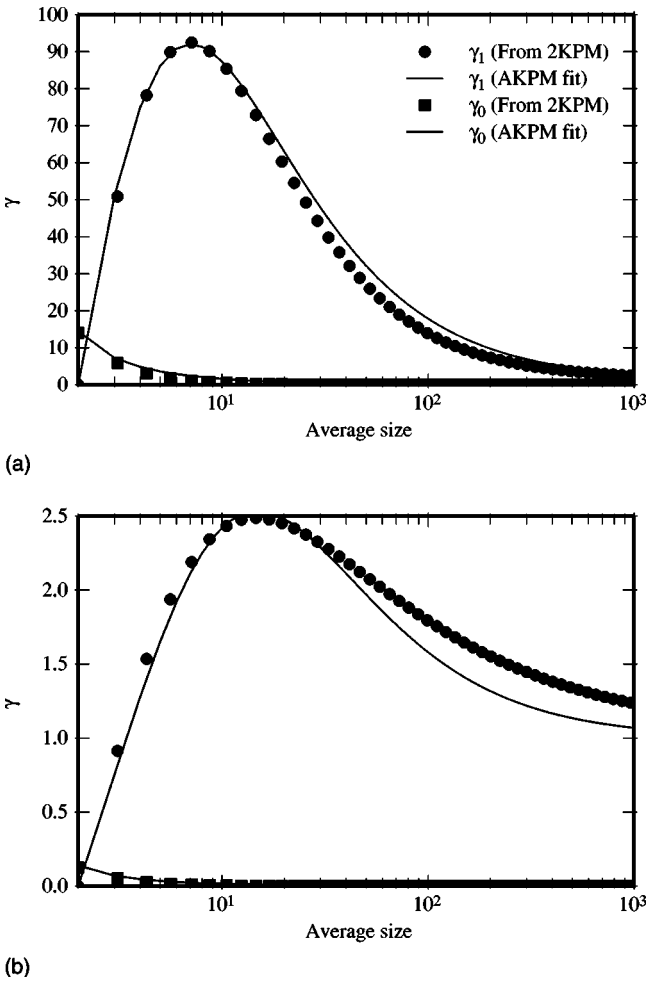

FIG. 2. Values of γ_0 (■) and γ_1 (●), as calculated from Eq. (10) and as fitted by AKPM functions [Eq. (14)]. The $\Delta G_n^{\mathrm{exc}}$ parameters and the corresponding parameters for γ_i are (a) $a_0 = 3.855$, $a_1 = 15.9$, $a_2 = -1.4$, with $K_0 = 3$, $K_1 = 14.5$ and $K_2 = 366$. (b) $a_0 = 1$, $a_1 = 4.7$, $a_2 = 0$, which correspond to $K_0 = 8$, $K_1 = 0.14$, and $K_2 = 8$.

Note that the approximations have the right asymptotic behavior as given in Eq. (13).

Since the γ_i calculated from 2KPM and determined by the analytical functions of AKPM are approximately equal, we would expect that both models would give the same simulation results. Indeed, when we test both models under the same conditions, the results are almost indistinguishable (Fig. 3). To obtain Fig. 3, we have used the parameters of Fig. 2(a), with an initial 5×10^{13} cm^{-2} interstitial dose.

It is also possible to find $\hat{C}_n^*$, and hence $\Delta G_n^{\mathrm{exc}}$, if the fitting parameters of γ_i (namely, K_i) and the distribution function ($\hat{f}_n$) are given, although this procedure is less straightforward. Since γ_0 is the product of $\hat{C}_1^*$ and $\hat{f}_2$, knowing γ_0, we can easily find $\hat{C}_1^*$. On the other hand, γ_1 is dependent on $\hat{C}_2^*$ through $\hat{C}_\infty^*$. So we can find $\hat{C}_n^*$ by solving a large set of linear equations defined by

$$\gamma_1(\hat{m}_1) = \sum_{n=2}^{\infty} \hat{C}_n^* \hat{f}_{n+1}(\hat{m}_1) \tag{17}$$

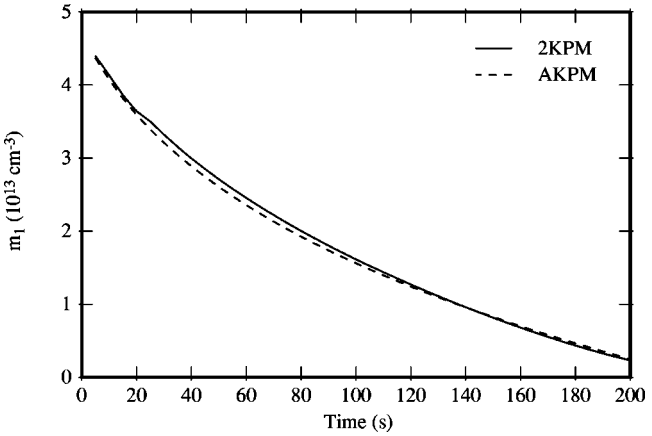

FIG. 3. Comparison of 2KPM and AKPM under identical implant and anneal conditions where equivalent parameters as given in Fig. 2(a) are used.

at different $\hat{m}_1$. Once $\hat{C}_n^*$ is determined, ΔG_n^{exc} can be found by solving the expression for C_n^* [Eq. (3)] for ΔG_n^{exc}, which gives a recurrence relation:

$$\Delta G_{n+1}^{\text{exc}} = \Delta G_n^{\text{exc}} + kT \ln \hat{C}_n^* . \tag{18}$$

Obviously, ΔG_1^{exc} must be defined as a reference point.

IV. COMPARISON OF MODELS TO EXPERIMENTAL DATA

In this section, we compare four extended defect models: a three-moment model (3KPM) which was demonstrated in our previous work,[1] the two-moment model (2KPM) described above, a one-moment or simple solid solubility (SSS) model, and the AKPM described above. We first review the assumptions of these four models:

(1) One-moment model (SSS): In this model, we assume that solute atoms above solid solubility precipitate to extended defects with a diffusion limited rate. This model does not account for Ostwald ripening.
(2) Two-moment model (2KPM): We use log-normal distribution of extended defects with fixed z_2. The variables we have are m_0 and m_1.
(3) Three-moment model (3KPM): We use an energy minimizing closure assumption with three moments.
(4) Analytical model (AKPM): We use analytical functions for the reaction rates that depend on average size.

Figure 4 shows the comparison of one-, two- and three-moment models to the {311} dissolution data from Eaglesham *et al.*[5] It can be observed that both the two- and three-moment models accurately capture the observed behavior. However, the one-moment model cannot account for the exponential decay in the number of interstitials stored in {311} defects. Since it neglects the Ostwald ripening process, it predicts an approximately linear decay in the number of interstitials stored in {311} defects. The exponential decay rate is mainly a result of decreasing supersaturation of interstitials with time, which is, in turn, a result of the increase in average size of the extended defect population and the decrease in the number of extended defects remaining.

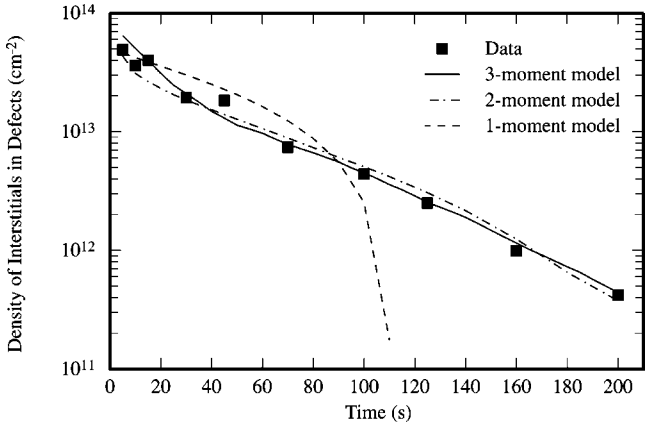

FIG. 4. Comparison of one-, two-, and three-moment models for evolution of {311} defects. Both two- and three-moment models capture the exponential decay of interstitials in {311} defects as observed by Eaglesham *et al.* (see Ref. 5).

When we apply AKPM to the same set of data, we find that it also describes the Ostwald ripening process equally well (Figs. 5 and 6). Note that the model parameters are calibrated using only the experimental data in Fig. 5, and hence Fig. 6 shows the prediction of the model for the Ostwald ripening process and is not a curve fit. Thus, the good agreement in the average {311} defect size further validates the modeling approach.

We find that the computation time with the AKPM model is much smaller than the computation time of the RKPM model. This makes AKPM the model of choice for simulation of {311} defects in large systems. The fact that AKPM does not require any proprietary operators enables easy integration into many PDE solvers.

If we look at TED data from Packan,[6] the differences between the three models is relatively small (Fig. 7). One can readily observe that the final amount of TED predicted by all three models is approximately the same. For large thermal budgets at constant temperature, as is the case with this data, all extended defects created by the implant damage are dissolved. In such a case, the amount of TED depends

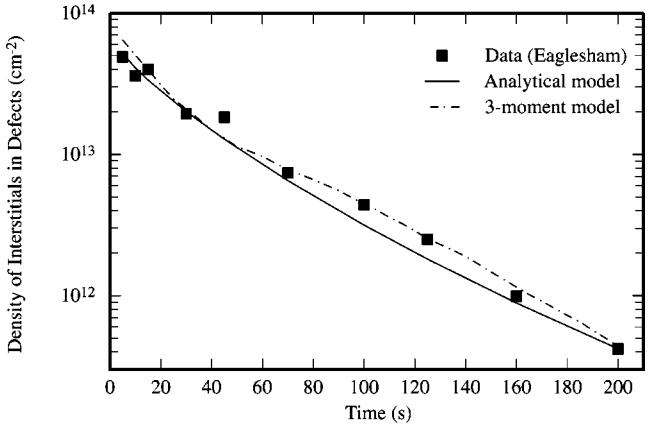

FIG. 5. Evolution of density of interstitials in {311} defects (m_1) from Eaglesham *et al.* (see Ref. 5) and comparison to the analytical model (AKPM) and three-moment model (3KPM).

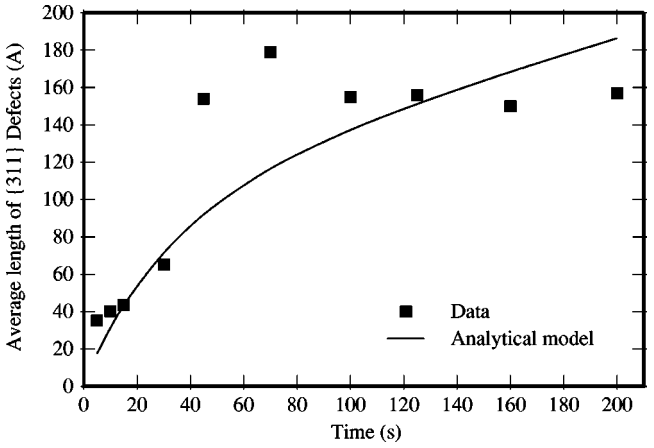

FIG. 6. The analytical model's (AKPM) prediction of the evolution of the average length of {311} defects and comparison to data from Eaglesham *et al.* (see Ref. 5).

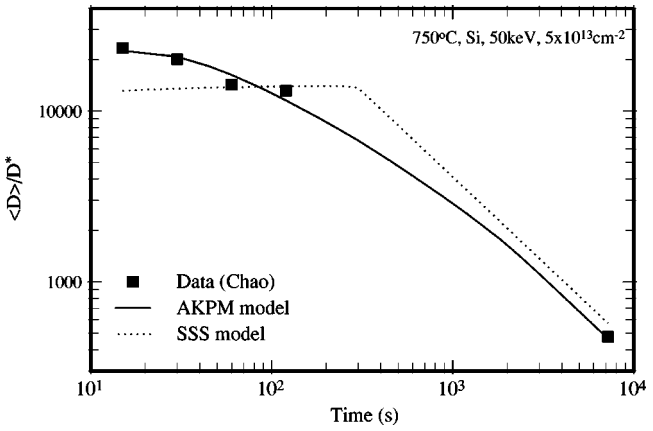

FIG. 8. Comparison of one- and two-moment models for short-time diffusivity enhancements. Data from Chao (see Ref. 7) for a 5×10^{13} cm^{-2} 50 keV implant with anneals at 750 °C.

only on how much the initial damage was and how effective the surface is in terms of consuming interstitials. Therefore, all three models give similar results.

However, before the damage is completely annealed and while the interstitial super-saturation is still evolving, we expect significant differences between the models. Indeed, if we look at short-time behavior more closely using data from Chao,[7] the difference between the models becomes evident (Fig. 8). The one-moment model predicts a constant enhancement of diffusivity until TED is over, whereas the two-moment model accounts for the reduction of diffusivity enhancement—or interstitial supersaturation—during TED. Again, this is an effect caused by the Ostwald ripening process. These differences in TED kinetics play an important role in the final amount of diffusion when TED occurs over more than one temperature, such as for spike anneals where most of the diffusion occurs during the ramp up.[8]

V. COMBINED ANALYTICAL DISLOCATION LOOP AND {311} DEFECT MODEL

As a next step, we seek to find an analytical model for loop evolution based on the analytical model for {311} defects (AKPM) and combine these two models in one. We assume that {311} defects transform into dislocation loops by an unfaulting reaction once they reach a critical size.[9,10] This process has been observed experimentally via *in situ* TEM.[11] For a more detailed discussion of the loop formation process, please refer to Ref. 4.

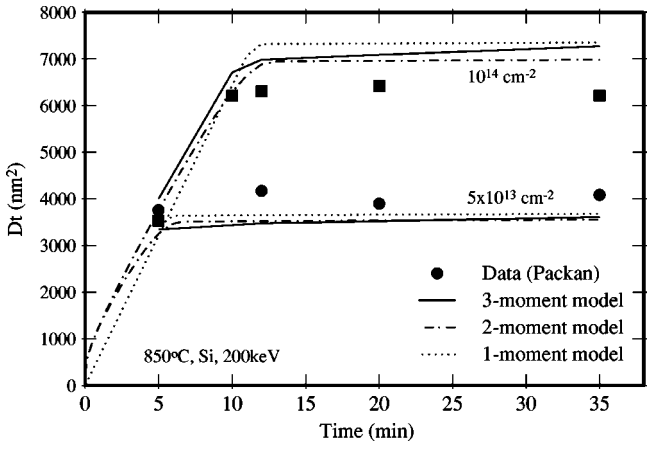

FIG. 7. Comparison of one-, two-, and three-moment models for TED predictions. The models differ significantly only at short-time behavior, which this data (Packan, see Ref. 6) cannot distinguish.

We can note the following points for the functions that are involved in AKPM:

(1) Loops have a lower solid solubility than {311} defects, typically close to C_I^*. Therefore, we have to set the solid solubility of the {311} defects/dislocation loop distribution to C_{ss}^{loop}. Since the γ_i are inversely proportional to the solid solubility, the values determined from {311} defects have to be multiplied by the C_{ss} ratio.
(2) To ensure $\lim_{n\to\infty}\gamma_1=1$, we need a functional change after the {311}/loop crossover point (n_{crit}).
(3) The γ_i have to be continuous at the {311}/loop crossover point (n_{crit}).

To understand what type of function these restrictions give, we proceed as earlier. We use ΔG_n^{exc} for the joint population of {311} defects and dislocation loops, which is identical to ΔG_n^{exc} for {311} defects at sizes smaller than n_{crit}, except for an offset due to C_{ss} difference (a_3 term), and is proportional to the loop perimeter ($\propto n^{0.5}$) for sizes larger than n_{crit}:[9,10]

$$\Delta G_n^{exc}=\begin{cases} a_0 n^{\beta_0}+a_1 n^{\beta_1}+a_2 n^{\beta_2}+a_3 n & \text{for } n<n_c, \\ b_0 n^{0.5}+b_1 & \text{for } n\geqslant n_c. \end{cases} \tag{19}$$

Together with a log-normal distribution function we find the corresponding γ_i as we did for {311} defects by Eq. (10). The results are shown in Fig. 9, together with analytical functions that capture the behavior of γ_1.

We find a set of γ_i functions to be used with AKPM by extending the set of functions we used for {311} defects:

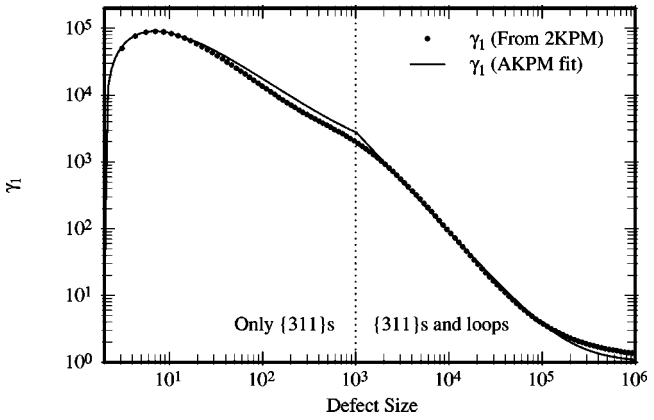

FIG. 9. The γ_1 function for both {311} defects and dislocation loops as derived from ΔG_n^{exc} and a log-normal closure assumption. For $\hat{m}_1 < n_{\text{crit}}$, γ_1 is identical to that for {311} defects, except for a multiplier to account for differences in solid solubility.

$$\gamma_0 = \begin{cases} \dfrac{C_{\text{ss}}^{\{311\}}}{C_{\text{ss}}^{\text{loop}}} \dfrac{K_1}{\hat{m}_1 - 1} & \text{for } \hat{m}_1 < n_{\text{crit}}, \\ K_3 \left(\dfrac{1}{\hat{m}_1 - 1} \right)^{\alpha} & \text{for } \hat{m}_1 > n_{\text{crit}}, \end{cases} \tag{20}$$

$$\gamma_1 = \begin{cases} \dfrac{C_{\text{ss}}^{\{311\}}}{C_{\text{ss}}^{\text{loop}}} \dfrac{\hat{m}_1 - 2}{\hat{m}_1 + K_0} \left(1 + \dfrac{(K_0+2)K_2}{\hat{m}_1 + K_0} \right) & \text{for } \hat{m}_1 < n_{\text{crit}}, \\ 1 + K_4 \left(\dfrac{K_0 + 2}{\hat{m}_1 + K_0} \right)^{\alpha} & \text{for } \hat{m}_1 > n_{\text{crit}}, \end{cases} \tag{21}$$

where K_3 and K_4 are chosen such that continuity of γ_0 and γ_1 are ensured. In our simulations, we have used a crossover point of $n_{\text{crit}} = 1000$ and left α as a fitting parameter. Please note that n_{crit} should not be interpreted as "the point where the {311} defect to dislocation loop transformation happens," but rather "the size below which no {311} defect to dislocation loop transformation happens." The transformation will occur at any size greater than n_{crit}.

We again compare our model against data from Pan *et al.*[12] As one can readily observe, a good match can be found (Figs. 10 and 11). The model also captures the Ostwald ripening process of dislocation loops (Fig. 11). Since this model does not explicitly distinguish between the interstitials contained in dislocation loops and the interstitials contained in {311} defects, we can not plot them separately. However, to obtain an idea of how the {311} defects would evolve, we can turn off the loop portion of the model and plot {311} defects in the absence of loops (Fig. 10).

As a check of the predictive capabilities of the unified {311} defect/dislocation loop model, we have resimulated the data by Packan[6] with the dislocation loop model turned on. Since the model is analytic, and only the functions are different, there is no significant speed penalty associated with including the loop model along with the {311} defect model. The results are depicted in Figs. 12 and 13. Since all implants in this data set were under subamorphizing conditions, there is no significant difference between the {311} defect model and the unified model, except for the highest doses and energies. The model predicts that at higher doses and energies, where TED lasts longer, a significant portion of the {311} defect population turns into dislocation loops. Since loops sustain a smaller supersaturation than {311} defects, this reduces the total amount of TED for higher doses and energies, resulting in a better match with the experimental data.

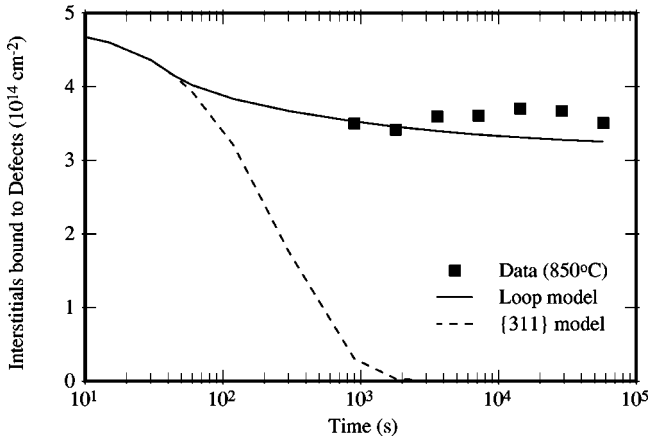

FIG. 10. Evolution of the total number of interstitials stored in dislocation loops and {311} defects for the AKPM. Data for 1×10^{16} cm^{-2} Si implant at 50 keV with anneal at 850 °C from Pan *et al.* (see Ref. 12).

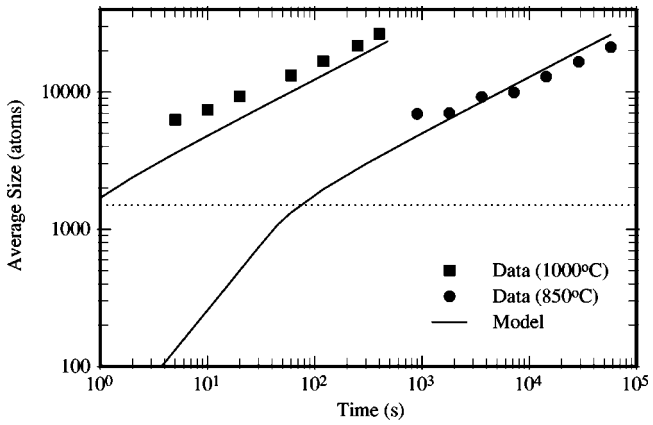

FIG. 11. Evolution of average defect size for 1×10^{16} cm^{-2} Si implants at 50 keV from Pan *et al.* (see Ref. 12) compared to the prediction of AKPM.

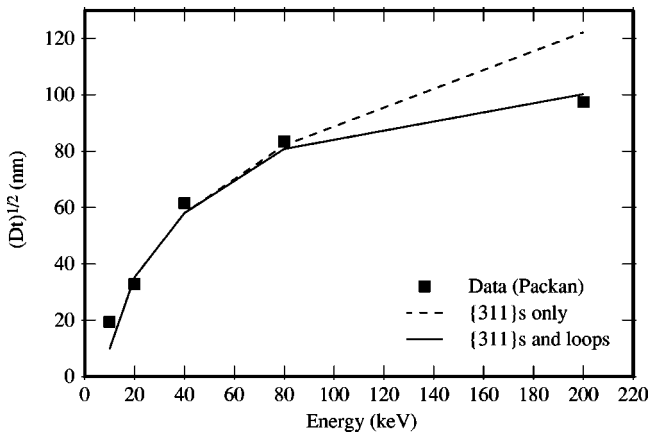

FIG. 12. Prediction of the energy dependence of TED using the unified loop/{311} defect model. Data from Packan (see Ref. 6).

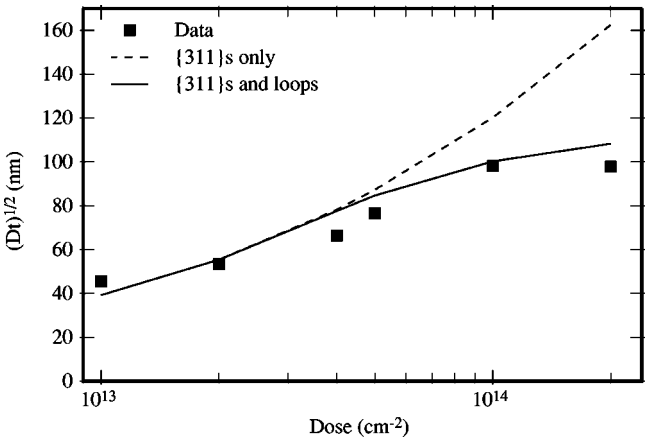

FIG. 13. Prediction of the dose dependence of TED using the unified loop/{311} defect model. Data from Packan (see Ref. 6).

VI. SUMMARY

We presented an alternative formulation of a previous moment−based model for extended defect kinetics, which is more efficient and does not require lookup tables. The infinite nonlinear sums in previous model (RKPM) can be represented by analytical functions with new fitting parameters without loss of generality. The new formulation can be implemented in any PDE solver, without the need for special operators and can be used in multidimensional simulations without a large performance penalty. The model has been successfully calibrated to the evolution of {311} defects following ion implantation.

We have also presented an extension of the same model to dislocation loop formation from {311} defect unfaulting. This extension results in a unified model that accounts for the nucleation, growth, transformation, and dissolution of {311} defects and dislocation loops. Via application of this model, we also demonstrated that loop formation can effect TED significantly for high dose and energy implants, even when the implants are subamorphizing.

[1] A. H. Gencer and S. T. Dunham, J. Appl. Phys. **81**, 631 (1997).
[2] I. Clejan and S. T. Dunham, J. Appl. Phys. **78**, 7327 (1995).
[3] G. Z. Pan and K. N. Tu, J. Appl. Phys. **82**, 601 (1997).
[4] A. H. Gencer, Ph.D. thesis, Boston University, 1999.
[5] D. J. Eaglesham, P. A. Stolk, H. J. Gossmann, and J. M. Poate, Appl. Phys. Lett. **65**, 2305 (1994).
[6] P. A. Packan, Ph.D. thesis, Stanford University, 1991.
[7] H. S. Chao, Ph.D. thesis, Stanford University, 1997.
[8] S. T. Dunham, S. Chakravarthi, A. H. Gencer, and D. F. Downey, in *Si Front-End Processing—Physics and Technology of Dopant-Defect Interactions II*, edited by H-J. L. Grossmann, T. E. Haynes, M. E. Law, A. N. Larsen and S. Odanaka, Mater. Res. Soc. Symp. Proc. Proceedings No. **568** (Materials Research Society, Pittsburgh, 1999).
[9] A. H. Gencer and S. T. Dunham, in *Microstructure Evolution During Irradiation*, edited by I. M. Robertson, G. S. Was, L. W. Hobbs, and T. Diaz de la Rubia, Mater. Res. Soc. Symp. Proc. Proceedings No. **439** (Materials Research Society, Pittsburgh, 1997).
[10] A. H. Gencer and S. T. Dunham, in *Materials Modification and Synthesis by Ion Beam Processing*, edited by D. E. Alexander, N. W. Cheung, B. Park, and W. Skorupa, Mater. Res. Soc. Symp. Proc. Proceedings No. **438** (Materials Research Society, Pittsburgh, 1998).
[11] J. Li and K. S. Jones, Appl. Phys. Lett. **73**, 3748 (1998).
[12] G. Z. Pan, K. N. Tu, and S. Prussin, Appl. Phys. Lett. **68**, 1654 (1996).